POLITECNICO
MILANO 1863

SCUOLA DI INGEGNERIA INDUSTRIALE
E DELL'INFORMAZIONE

Executive Summary of the Thesis

Mesh morphing for CFD applications

Laurea Magistrale in Energy Engineering - Ingegneria Energia

Author: Vishal Garg

Advisor: Prof. Fabio Inzoli

Co-advisor: Prof. Federico Piscaglia, Dr. Konstantinos Gkaragkounis (Optimad Srl)

Academic year: 2022-2023

1. Introduction

The role of quality of dynamically updated 3D meshes is quite important in the design and analysis of many engineering applications where the boundary between the fluid and the solid can have motion like aerodynamic shape optimization, fluid-structure interaction, moving boundary problem etc ([1], [2]). The design process of these dynamic CFD applications require new meshes in every design iteration. There exist mainly two kinds of methods to generate the new meshes for each design iteration. The first method is to regenerate the mesh after each iteration. Since the generation of mesh is a tedious task, it is very time expensive to recreate a good quality mesh after every design iteration, and therefore it is not the best method to carry on design iterations. Another shortcoming of re-meshing is in applications like aerodynamic optimization, where after each design step, the targeted field suffers from discretization errors. The second method to create the new mesh for the new design iteration is to morph the existing mesh. This method is hardly as time consuming but the quality depends on the technique used to morph the existing mesh. Another benefit of mesh morphing is the ease to achieve high-order accuracy in time because of the unchanged mesh topology with respect to the time steps.

In literature, numerous research has been carried out to morph the volumetric meshes ([3], [4]). There exist mainly two kinds of techniques to morph a target mesh namely; 1. Physical analogy based techniques and, 2. Interpolation based techniques. Among the physical analogy based techniques, there are spring based, elasticity based and Laplacian based techniques, whereas among the interpolation based techniques, there exist the Transfinite interpolation (TFI), Inverse distance weighting (IDW), Radial basis functions (RBF), Delaunay graph, Quaternions based etc. techniques.

Among the physical analogy based techniques, the linear elasticity based analogy is the most promising but the main challenges are the computational cost and optimization of the physical properties E and ν. As far as the interpolation based techniques are concerned, the RBF with greedy algorithm seems to be the well developed and best performing technique.

The linear elasticity analogy based mesh morphing technique has been widely studied in literature. From the existing literature of linear elasticity technique, it is evident that finding an optimum relation for the elasticity coefficient E and Poisson's ratio ν is still a challenge and hence required to be worked upon. In the field

of aerodynamic shape optimization, the contribution of the linear elasticity technique is not explored yet. Moreover, for the FSI applications, complex deformations for complex geometries are not studied well in detail. In literature, the results of the linear elasticity technique have not been compared with the results obtained using any other promising technique at any level of detail. Therefore, there exist the scope of not only finding the new relations for the elasticity coefficient and Poisson's ratio in the linear elasticity technique but also exploration of it's use in different CFD applications and comparisons of the results with the other different techniques. Driven by the promising nature of the linear elasticity technique, the related applications and possible improvements, the present thesis focuses on the development of the linear elasticity analogy based mesh morphing technique. The objective of the present study is to develop a robust and accurate mathematical model and find a global relation for the physical properties E and ν. A special emphasis is given to the accuracy of mathematical model at the boundaries. A second order accuracy is ensured throughout the mesh. A parametric study is conducted to see the effect of different parameters in the relations of E and ν on the quality of the mesh. The effect of different kinds of surface deformation on the optimum parameters is analysed too. Another objective of the present study is to apply the elasticity morpher to different kinds of industrial applications and check the quality of the deformed mesh under different kinds of extreme deformations that the industrial application might undergo. The results obtained by the linear elasticity morpher are also compared with the results obtained by the existing Laplacian and the Laplacian quaternions techniques which were available to the author. Throughout the study, efforts are made to increase the accuracy of the various computation terms.

2. Governing equations and mathematical model

An elastic solid subjected to body forces and surface traction undergoes deformation. In case of small deformations, it is possible to govern the behaviour of the solid using the law of linear elasticity. For a small displacement $U = (u, v, w)$ the equation of linear elasticity can be written as follows:

$$\nabla.\sigma = f \quad on\ \Omega, \tag{1}$$

Here, f is the body force, σ is the stress tensor, and Ω is the computational domain. The stress tensor σ can be described in terms of the strain tensor ϵ using the constitutive relation as follows:

$$\sigma = \lambda Tr(\epsilon)I + 2\mu\epsilon \tag{2}$$

where λ and μ are the Lamé constants and Tr is the trace. The Lamé constants are functions of the material properties Young's modulus E and Poisson's ratio ν as follows:

$$\lambda = \frac{\nu E}{(1+\nu)(1-2\nu)}, \qquad \mu = \frac{E}{2(1+\nu)} \tag{3}$$

The Young's modulus E shows the stiffness of the solid. A large E indicates that the solid is rigid, whereas a low E indicates more elastic nature. Poisson's ratio ν indicates the measure of deformation in lateral direction when the solid is undergone a deformation in the axial direction. The value of ν for physical materials can lie between $(-1, 0.5)$.
As per the linear kinematic law

$$\epsilon = \frac{1}{2}(\nabla U + \nabla U^T), \tag{4}$$

describes the change in length and orientation of an element in the solid. For rigid body rotations, an alternative relation for the Lamé constants is suggested in a study by Dwight [5] by making the stress on the elements equal to 0 instead of the ones derived from the elasticity equations. It is reported that a better mesh quality is obtained for not only the rigid body rotation cases but all the other applications in general. These alternative Lamé constants are shown hereby:

$$\lambda = -E, \qquad \mu = E, \tag{5}$$

In present work, these alternative Lamé constants are inspected along the ones obtained from the elasticity equations. As far as boundary conditions are concerned, one of the possibility over the boundary surface can be the Dirichlet boundary condition given by $U = U_b$ in $\partial\Omega$. In literature there have been various ways of computing the elasticity Coefficient E and the Poisson's ratio ν. Among the relations proposed, the relation of E inversely proportional

to the volume of the cell is widely accepted and used [4], with ν kept as a constant value between $(-1.0, 0.5)$. Given the agreement in literature, in present work, a variant of this relation is proposed and studied. This new relation is shown as follows:

$$E_{Cell} = \frac{1}{(V_{Cell})^p}, \tag{6}$$

Where, E_{Cell} and V_{Cell} are the elasticity coefficient and volume of the concerned cell, and p is an exponent to the inverse of volume of the cell. Exponent p helps in providing the cells close to the boundary, which have smaller volume with respect to the cells far from the boundary, with considerably high stiffness which in turn helps these cells in preserving their shape. Another widely used relation for E keeping the ν constant is inverse of distance from the boundary. In present work, a variant of this relation is proposed and studied. This new relation is as follows:

$$E_{Cell} = \frac{1}{(d_{Cell})^q}, \tag{7}$$

Where, d_{Cell} is the distance of the concerned cell centroid from the nearest boundary point , and q is an exponent to the inverse of this distance. Just like p, exponent q helps in providing the cells close to the boundary, which have smaller d_{Cell} with respect to the cells far from the boundary, with considerably high stiffness which in turn helps these cells in preserving their shape.

In present work, equation of linear elasticity is discretized using a finite volume method (FVM) and solved using a PETSc library. The FVM discretization is done based on field variables at the cell centers. Using Eqs. 2 and 4, Eq. 1 can be rewritten in the following Einstein form:

$$\frac{\partial}{\partial x_i}\left[\lambda \frac{\partial u_k}{\partial x_k} I_{ij} + \mu\left(\frac{\partial u_i}{\partial x_j} + \frac{\partial u_j}{\partial x_i}\right)\right] = f_i \tag{8}$$

This system of equation needs boundary conditions to be solved. This boundary condition in case of the equation of linear elasticity can be Dirichlet kind or the Neumann kind based on the boundary information provided. It is to be noticed that the equation of linear elasticity is valid only for small deformations, and therefore, a multi-step approach is used to allow the linear elasticity equations to be applicable to the large deformations. The algorithm used in the present work is shown in Algorithm 1.

Algorithm 1 Solution algorithm for the elasticity solver with multi-step.

1: Setup the solver: Initial geometry, boundary displacements on nodes, relaxation factor
2: Interpolate displacements from boundary nodes to boundary face centers
3: Computation of the cell and face gradient stencils
4: Computation of the Lamé constants
5: Computation of the Laplacian stencils
6: Initial guess for the displacements in the bulk mesh
7: Divide the boundary displacements by nsteps
8: Initialize the solver by passing the LHS
9: **for** $(istep = 0;\ istep < nsteps;\ istep++)$ **do**
10: **while** $max(residuals) < Tolerance$ **do**
11: Compute the cell and face gradients
12: Compute the source terms due to $Terma$ and $Termb1$
13: Compute the source term due to the contribution from Laplacian term
14: Compute the overall source term
15: Solve the linear system of equations using PETSc component by component
16: Compute the residuals using the new and old solutions
17: **end while**
18: Interpolate the obtained displacements from cell centers to nodes
19: Calculate the error between the boundary displacement provided and obtained from this step and propagate into the bulk mesh
20: Update the displacements in the bulk mesh
21: Apply the displacements on the bulk mesh and update the geometry
22: **if** istep < nsteps-1 **then**
23: Update the cell and face gradient stencils
24: Update the Lamé constants
25: Update the Laplacian gradient stencils
26: Update the LHS in the solver
27: **end if**
28: Compute the total displacement upto this step
29: Set the solution as the initial guess for the next step
30: **end for**
31: Restore the initial geometry
32: Restore the initial boundary condition
33: Final displacements

3. Results: A non-uniform cube

In present work, the results of the developed elasticity solver are demonstrated on a non-uniform cube with 64k cells by applying mainly two different and opposite kinds of boundary conditions; namely, outward and inward. In the outward kind of boundary condition, all the 6 faces of the cube are expanded by pivoting the center of the faces and pulling by a length 60% of the edge length of the cube. In the inward kind of boundary condition, the same faces are compressed by pivoting the centers of the faces and pushing by a length 25% of the edge length of the cube. To obtain the results in the present section, the elasticity coefficients are computed using an inverse of volume method as explained in Sec. 2 with exponent $p = 1$. In present work, because of the use of a FVM for discretization, the displacement field is computed at the cell centers and then interpolated to the nodes. The magnitude of the displacements obtained from the linear elasticity solver for an outward deformation at the cell centers are shown in the left of Fig 1. The displacement field at the cell centers increases from blue to red color. After interpolating the displacement field from the cell centers to the nodes and applying this displacement field on initial geometry, the final deformed geometry is obtained as shown in right of Fig 1. Similarly,

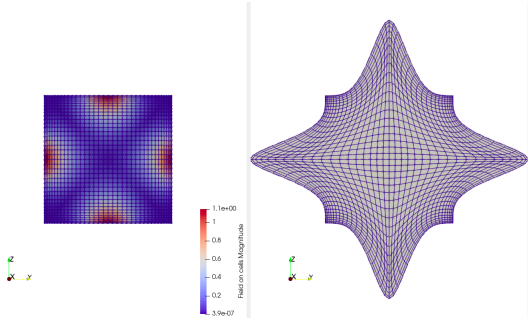

Figure 1: Mesh morphing for a cube with 64k cells: outward deformation.

for the inward deformation, the displacements on the cell centers and the final deformed mesh are shown in Fig. 2. For the cases of outward and inward deformations, it is observed that the boundary cells of the cube show the least shape change and hence preserve their shapes. This happens because of more stiffness at the cells close to the boundaries due to the low cell volumes near the boundaries. It is to be noticed

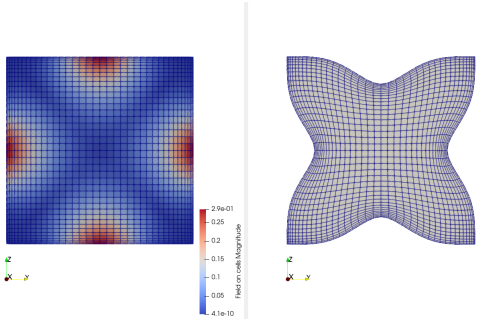

Figure 2: Mesh morphing for a cube with 64k cells: Negative deformation.

from the results that the orthogonality of the mesh near the boundary is very close to 90 deg, which shows a good quality of the mesh near the boundary. It can be also observed that the deformed mesh in both the outward and inward deformations is not in straight line but curved lines which means that the displacements in different dimensions are dependent. The reason for this behaviour of the deformed mesh is the coupled behaviour of the linear elasticity equation defined by a trace as shown in Eq. 8.

Deformation	**Max. non-orthogonality (deg.)**	**Max. boundary non-orthogonality (deg.)**	**Avg. non-orthogonality (deg.)**	**Max. skewness**
Outward	66.13	17.11	21.76	0.83
Inward	22.71	3.65	6.64	0.44

Table 1: Mesh quality in outward, inward and no deformation cases.

A table containing various mesh quality parameters for the outward and inward deformations is shown in Table 1. For a good quality mesh, the non-orthogonality at any interface should not be more than 70° which is satisfied by the results in Table 1. Additionally, positive minimum cell volumes and passed cell face validity are obtained which show that both the cases generate valid meshes for the applied displacements. For the mesh morphing applications as discussed in Sec. 1, the quality of the mesh at the boundaries should be good. It is evident from Table 1 for the present case of a non-uniform cube, that

the maximum non-orthogonality at the boundary comes out to be almost 17° and 3.5° for the outward and inward deformations respectively which show a good mesh quality.

3.1. Single vs multi-step approach

The present section describes the results for the case of a non-uniform cube using a multi-step approach. For the current study, 4 different number of steps are chosen and compared for both the outward and inward deformation boundary conditions. As per the discussion in Sec. 2, the Lamé constants are computed using an approach mentioned in Eq. 5 to consider the rigid body motion as well.
For both the outward and inward deformations, the non-uniform meshed cube is simulated with 1, 2, 5 and 10 steps. The results for these 4 different cases are shown in Fig. 3 and 4. In the case of an outward deformation, the effect of multi-step is not so clear in the cross section images, and therefore, a mesh quality Table 2 is shown for details on the quality of the mesh with the number of steps.

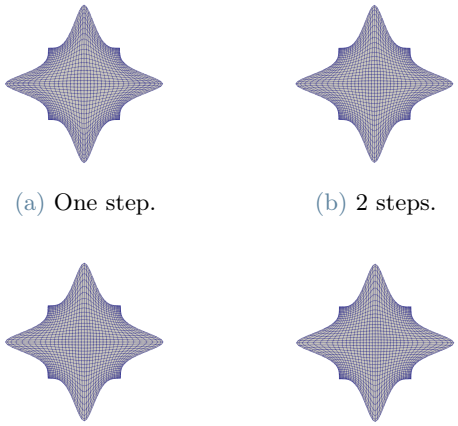

(a) One step. (b) 2 steps.

(c) 5 steps. (d) 10 steps.

Figure 3: Outward deformation using the multi-step approach as shown in Sec. 2.

It can be observed in Table 2 that the maximum non-orthogonality does not change much but the average non-orthogonality decreases considerably by increasing the number of steps. It can be also observed that the maximum non-orthogonality at the boundary decreases as well which is much needed improvement for mesh morphing applications. For all the cases with different number of steps, it is found that the

Steps	**Max. non-ortho-gonality (deg.)**	**Max. boundary non-ortho-gonality (deg.)**	**Avg. non-ortho-gonality (deg.)**	**Max. skew-ness**
1	61.99	24.37	20.69	0.80
2	61.63	22.79	19.17	0.83
5	62.01	22.02	18.03	0.85
10	61.95	21.65	17.58	0.86

Table 2: Mesh quality in outward deformation with different number of steps.

minimum cell volume is positive and all the cell face validity are passed which indicate that all the deformed meshes remain valid. It is to be noticed that the skewness increases with the increase in number of steps but the extent of increase is not considerable with respect to the betterment in the non-orthogonality and a trade-off benefits the high number of steps.
For an inward deformation, all the 6 faces of the cube are pushed by a length equal to 25% of the edge length of the cube with respect to 15% in the previous section to better show the impact of the multi-step approach. Unlike the outward deformations in Fig. 3, the effect of using a multi-step approach is clearly visible in Fig. 4. For such a high inward deformation, a single step approach as shown in Fig. 4a fails to provide a valid mesh. It can be seen that the

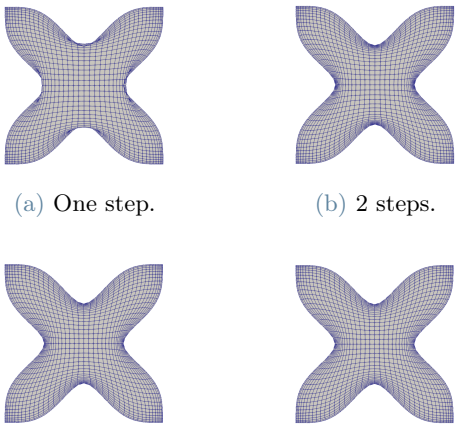

(a) One step. (b) 2 steps.

(c) 5 steps. (d) 10 steps.

Figure 4: Inward deformation using the multi-step approach as shown in Sec. 2.

nodes at and near the boundary intersect with the nodes in the bulk mesh. For steps 2-10 in Fig. 4, it can be observed that the congestion of the mesh near the boundary decreases with increase in number of steps, which indicates that the mesh near the boundary is preserving it's shape more for more number of steps. To look into further details, the mesh quality parameters are listed in Table 3 for a comparison between all the 4 cases.

Steps	**Max. non-orthogonality (deg.)**	**Max. boundary non-orthogonality (deg.)**	**Avg. non-orthogonality (deg.)**	**Max. skewness**
1	180.0	3.99	13.25	6.7
2	37.98	4.83	12.57	0.73
5	39.61	5.61	13.49	0.73
10	40.3	5.99	13.82	0.73

Table 3: Mesh quality in inward deformation with different number of steps.

For a single step approach, it is clear from Table 3 that the maximum mesh non-orthogonality of 180°, negative mesh volumes and a 0 cell face validity exist, which make the overall mesh invalid. For number of steps $2-10$ it is observed that the maximum and average non-orthogonality and maximum skewness increase slightly with the increase in number of steps. The reason behind this behaviour can be explained using Fig. 4 where it can be seen that the increase in number of steps decreases the congestion near the boundaries. Due to decrease in congestion near the boundaries, the mesh overall moves towards the center of the cube and because of the finite volume inside the cube, the average angle between the normal of a face and the vector connecting the two neighbour cell centers increases. The similar happens at the boundary, where the cells are more orthogonal when they are smaller and hence closer to each other but they become less orthogonal when the congestion reduces and cells try to preserve their original shape and hence farther from each other.
Overall, it can be said based on observations that a multi-step approach gives better results than a single-step approach in terms of mesh quality. Although the optimum number of steps can vary application to application. For applications with outward like deformations, clearly more number of steps help in providing better quality morphed mesh, but for inward like deformations, more number of steps helps in preserving the shape of the mesh close to the boundary but it hardly helps in enhancing the mesh quality parameters studied in the present work.

3.2. Parametric study

In present section, 2 different kinds of parametric studies are conducted; One on the Elasticity coefficient E, and the other on the Poisson's ratio ν. In the first kind of parametric study on elasticity coefficient E, 2 different relations to compute the elasticity coefficient are considered with two different parameters p and q respectively. In the second kind of parametric study, an optimum Poisson's ratio ν is found out by simulating the linear elasticity solver for different ν values. An outward and an inward kinds of deformations are considered for the simulations with a single step approach. A summary of the outcomes based on the parametric study conducted in the present chapter is listed as follows:

Elasticity coefficient E

- For any kind of deformation considered in this section, increasing the parameter p in the inverse volume relation or q in the inverse distance relation helps in preserving the mesh near the boundary but compresses the internal mesh far from the boundary resulting in clustering of cells.
- For an outward deformation, parameter $p = 0, 1, 2$ provides valid meshes in increasing order of mesh quality and parameter $q = 0, 1$ provides valid meshes with increasing order of mesh quality. When comparing the mesh quality tables, it is found that the inverse volume method with $p = 1, 2$ provides better results than inverse distance relation with $q = 1$. The parametric results for the case with inverse of volume method with the outward kind of deformation are shown in Fig. 5.
- For an inward deformation, a valid mesh is generated using $p = 3, 4$ with decreasing mesh quality and $q = 1$. The deformed mesh fails for $p = 0, 1, 2$ and $q = 0$ because

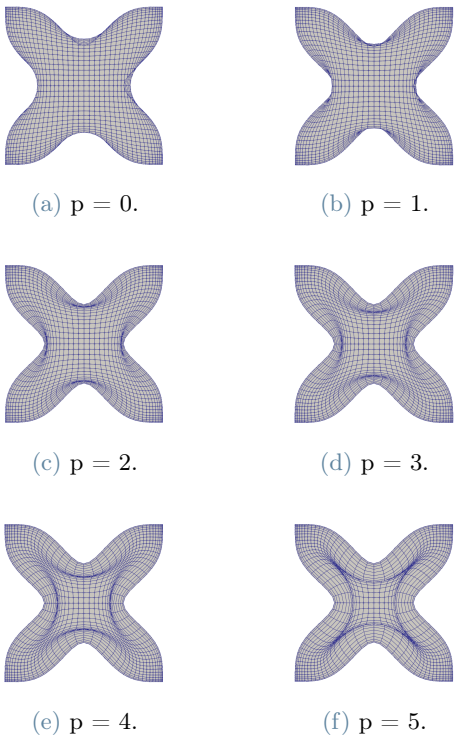

(a) p = 0. (b) p = 1. (c) p = 2. (d) p = 3. (e) p = 4. (f) p = 5.

Figure 5: Effect of inverse of volume exponent p on the Inward deformation.

of clustering and inversion of cells near the boundary and fails at $p = 5$ and $q >= 2$ due to clustering and inversion of cells far from the boundary. When comparing the mesh quality tables, $p = 3$ and $q = 1$ provide comparable mesh quality.

It is to be noted that the present parametric study is conducted over high deformations. There might exist small deformations where all the relations are able to provide with a valid mesh. The optimum choice of the parameters p and q depends on the kind of deformation provided as well.

Poisson's ratio ν

- Despite the possible upper limit of the Poisson's ratio ν being 0.5, a converged solution is obtained only until a maximum of 0.3 for both the outward and the inward kinds of deformations.
- For both kinds of deformations, a Poisson's ratio $\nu > 0$ generates the mesh with optimum mesh quality.

3.3. Comparisons with Laplacian and quaternions methods

In this section, the developed linear elasticity solver is compared with some of the promising existing mesh morphing techniques; namely, Laplacian and Laplacian quaternion techniques each with and without the narrow band width. The results of all the techniques are compared for a single as well as multi-step approaches. For an outward deformation with a single step approach, the results are compared in Fig. 6.

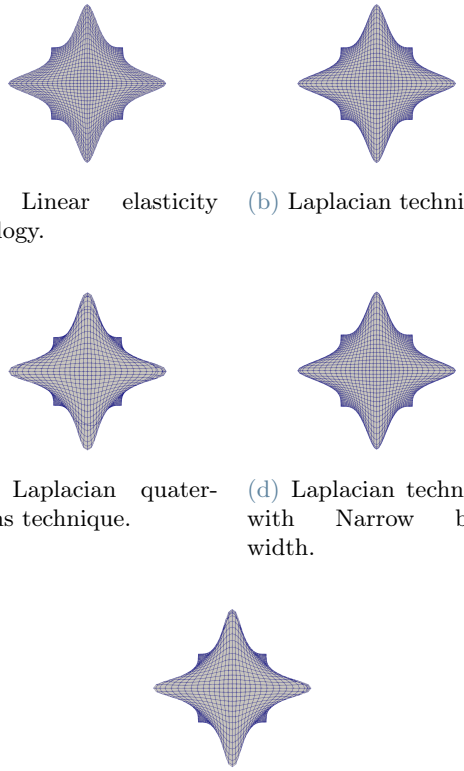

(a) Linear elasticity analogy. (b) Laplacian technique. (c) Laplacian quaternions technique. (d) Laplacian technique with Narrow band width. (e) Laplacian quaternions technique with Narrow band width.

Figure 6: Outward deformation in the cube with a single step approach.

For a single step approach, irrespective of the kind of deformation, the linear elasticity solver clearly provides results with much better mesh quality. The boundary mesh is preserved in a much better way in the solution of linear elasticity solver. The linear elasticity technique outperforms all the other techniques in all the mesh quality parameters. In a similar comparison for a multi-step approach, the linear elasticity technique clearly outperforms the Laplacian tech-

nique for any kind of deformation with or without the narrow band width. For a multi-step approach, for an outward deformation, the linear elasticity technique provides better results in the bulk mesh than the Laplacian quaternion technique with or without the narrow band width, but the Laplacian quaternion techniques with and without the narrow band width provides with better results at the boundary. For a multi-step approach with an inward deformation, the mesh quality comes out to be comparable for the linear elasticity technique and the Laplacian quaternion technique with or without the narrow band width. The narrow band width improves the mesh quality for both the outward and inward deformations at the boundary but worsen the mesh quality in the bulk mesh.

4. Industrial cases

Mesh morphing has various applications in the field of aerodynamic shape optimization, FSI, moving boundary problem etc. as discussed in Sec. 1. These wide field of applications provide the opportunity to apply the presently developed linear elasticity mesh morpher on the meshes undergoing such applications and test the quality of the output mesh. So far, the developed linear elasticity mesh morpher is tested only on a non-uniform cube with 64k cells. To test the robustness of the presently developed linear elasticity technique, two industrial cases from two different application fields are considered as follows:

- Wing of an airplane: FSI application
- Aerodynamic shape optimization in a car

4.1. Wing of an airplane

In present subsection, the industrial case of the wing of an airplane is considered. Unlike the non-uniform cube, where only the structured mesh with hexahedron kinds of cells was used, the wing contains a totally unstructured mesh with tetrahedron and hexahedron both kinds of cells. The mesh of the wing contains over 1.25 million cells including a symmetry plane. For the possible deformations under a turbulence like situation, it is found that the wing can withstand a linear bending upto 34°, non-linear bending upto 47°, twisting upto 47°, cambering upto 55°, and bending + twisting of upto 51°. By increasing the angle of bend or twist more than the limits just mentioned, the mesh fails due to a high maximum cell non-orthogonality (>85°) for the bending and bending + twisting cases and due to a high maximum boundary non-orthogonality for the twisting case. The cambering deformation fails because of the max. non-orthogonality and cell face validity crossing the respective limits and a negative cell volume altogether. The case with bending + twisting kind of deformation is shown in Fig. 7. The various mesh quality parameters for the comparison of different angles of deformation are plotted in Fig. 8.

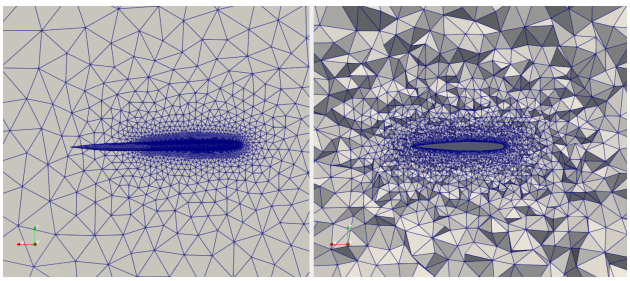

(a) Undeformed mesh.

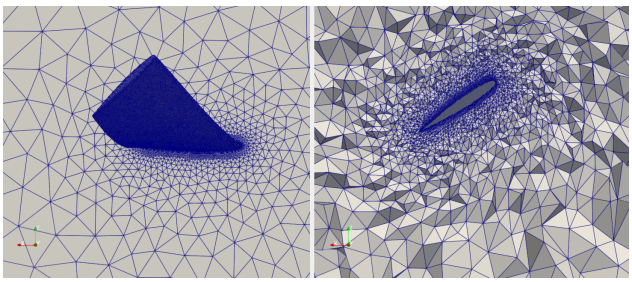

(b) Non-linear bend + twist of 50°.

Figure 7: Non-linear bending + twisting in a wing.

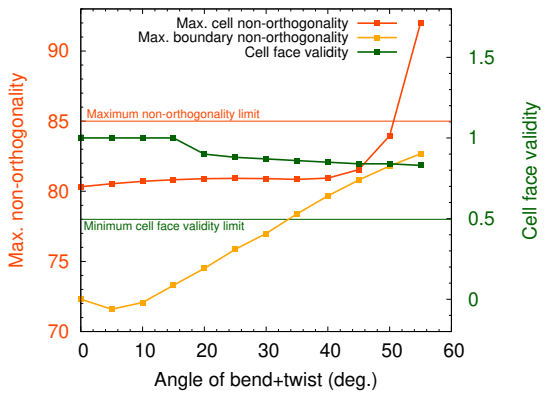

Figure 8: Mesh quality plot for a bend + twist in the wing of an airplane.

These case studies are performed with using the

Laplacian and Laplacian quaternion techniques and a comparison is made with the presently developed linear elasticity model. The results show that the maximum possible bend, twist or camber with a valid mesh with the use of the linear elasticity technique are of the order to that when using the Laplacian quaternions technique, whereas the linear elasticity solver outperforms the Laplacian quaternions technique for a relatively complex non-linear bending + twisting kind of deformation.

4.2. Aerodynamic shape optimization in a Car

In present section, the industrial case of a car is considered as shown in Fig. 9a. The mesh for the car consists of almost 2 million cells with polyhedral shape. To obtain the boundary deformation as the boundary condition, a RBF parameterization technique is used. The deformation in the surface of the car considered in the present section is shown in Fig. 9b. For the surface deformation, 6 different kinds of deformations are provided at different parts of the car. These deformations are: front window angle change, rear window angle change, roof drop or change in roof angle, greenhouse angle change,

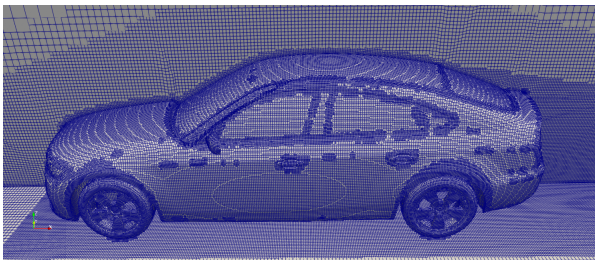

(a) Undeformed surface mesh.

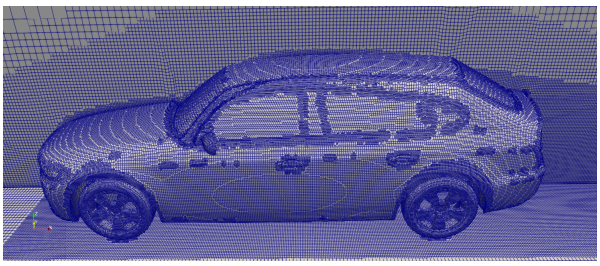

(b) Deformed surface mesh.

Figure 9: Surface deformation in the industrial case of a car.

front bumper nose extrusion, and front bumper nose drop. All these deformations can be observed in Fig. 9. It is to be noticed that the Dirichlet boundary condition is available only at the car surface and the walls of the CFD domain, and therefore, a slip condition is applied at the symmetry plane.

In present section, a multi-step approach with 5 steps is used to propagate the deformation in the volumetric mesh of the car. The elasticity coefficient E for the present section is computed using the relation with the inverse of volume with an exponent $p = 1$. The volumetric mesh displacement is demonstrated by showing a plane parallel to the symmetry plane for the initial and final geometries as shown in Fig. 10.

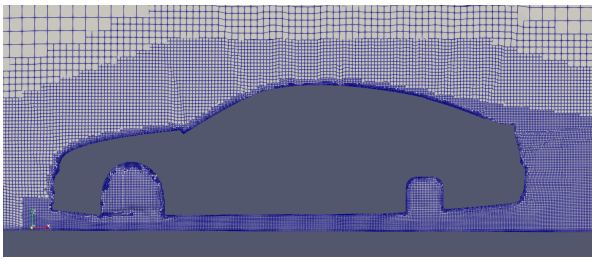

(a) Undeformed mesh.

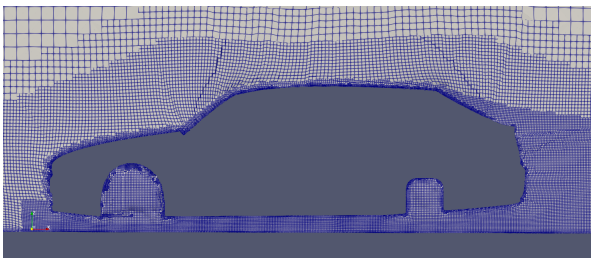

(b) Deformed mesh.

Figure 10: Volumetric mesh at a plane parallel to the symmetry plane.

It is evident from the results that the present linear elasticity based technique can morph the high deformation provided in the design of the car. The results for the present industrial case are compared also with the results obtained using a multi-step approach Laplacian quaternions technique. It is found in the comparisons that the presently developed linear elasticity technique provides with much better mesh compared to the Laplacian quaternions technique.

It is to be noticed for both the wing and the car industrial cases that the mesh near the boundary preserved their respective shapes despite high deformations and make the presently developed linear elasticity technique a robust tool to deform the meshes with high deformations thanks to the multi-step approach.

5. Conclusions and discussion

In present thesis, a mesh morpher based on the linear elasticity analogy is developed to propagate the surface deformation in the volumetric mesh. A FVM is used to descritize the PDEs and a PETSc library is used to solve the linear system of equations. While computing the cell and face gradients using a 2nd order least square method, the missing boundary contributions in the original method are also considered in order to keep the 2nd order of accuracy throughout the domain including the boundary and it is found that the added boundary contributions improve the accuracy of the cell and face gradients. Since the linear elasticity law is defined for small displacements, a multi-step step approach is developed where the solution geometry of the previous step is used as the initial geometry of the next step. For various geometries in general, it is found that the quality of the resulted mesh improves with an increase in the number of the steps in the multi-step approach.

A variation of two of the pre-existing relations for the computation of the elasticity coefficient E is proposed and analyzed in the present work. It is observed that the optimum values of the parameters used in these relations depend on the kind of deformation and the complexity of the mesh, which opens up a future opportunity to develop a method with the use of the introduced parameters depending on the type, size and location of the mesh control volume element.

The developed linear elasticity technique is tested for two different CFD applications, FSI and aerodynamic shape optimization, by means of two different industrial cases with much more complex and different kinds of meshes than the non-uniform cube. The first industrial case of the wing of an airplane contained tetrahedral and hexagonal mesh cells and tested over different kinds of deformations inspired by the turbulence event and aerodynamic shape optimization. It is observed that the presently developed linear elasticity solver is able to solve the high deformation provided to the wing and the car without any negative cell volume or cell inversion. The cells near the boundary of the car preserve their shape due to high stiffness caused by newly introduced relations for the elasticity coefficient E.

In a comparison of the results obtained using the presently developed linear elasticity technique with the promising techniques such as the Laplacian technique and the Laplacian quaternions technique with and without a narrow band width for single and multi-step approaches, it is found for the initial geometry of a non-uniform cube, that the linear elasticity technique clearly outperforms the Laplacian technique with and without the narrow band width, whereas the Laplacian quaternions technique produces comparable results with the linear elasticity technique. For the complex initial geometries of a wing and a car, for simple kinds of deformations, the linear elasticity technique can generate a valid mesh up to same order of respective deformation as with Laplacian quaternions technique, whereas the linear elasticity technique outperforms the Laplacian quaternions technique for a relatively complex deformation.

Therefore, based on the results of the non-uniform cube, the wing of an airplane and the car, it can be said that the presently developed multi-step approached linear elasticity solver provides with the best results compared to the Laplacian and Laplacian quaternions techniques with and without the narrow band width. This shows and affirms that the presently developed linear elasticity based mesh morpher can be used for the FSI, aerodynamic shape optimization and all the other kinds of CFD applications where mesh morphing is required.

6. Acknowledgements

I would like to take this opportunity to thank my supervisor **Konstantinos Gkaragkounis** (Senior engineer, Optimad Srl) and all the Optimad Srl team for their constant support and valuable guidance throughout the internship period. I would like to address my gratitude towards my professor guide **Prof. Fabio Inzoli** (Politecnico di Milano) and **Prof. Federico Piscaglia** (Politecnico di Milano) for their valuable feedback and advise throughout the thesis work.

References

[1] O Hassan, EJ Probert, and K Morgan. Unstructured mesh procedures for the simulation of three-dimensional transient compressible inviscid flows with moving boundary components. *International journal for*

numerical methods in fluids, 27(1-4):41–55, 1998.

[2] Hong Fang, Chunye Gong, Caihui Yu, Changwan Min, Xing Zhang, Jie Liu, and Liquan Xiao. Efficient mesh deformation based on cartesian background mesh. *Computers & Mathematics with Applications*, 73(1):71–86, 2017.

[3] Keith Stein, Tayfun Tezduyar, and Richard Benney. Mesh moving techniques for fluid-structure interactions with large displacements. *J. Appl. Mech.*, 70(1):58–63, 2003.

[4] MM Selim and RP Koomullil. Mesh deformation approaches–a survey. *Journal of Physical Mathematics*, 7(2):1–9, 2016.

[5] Richard P Dwight. Robust mesh deformation using the linear elasticity equations. In *Computational fluid dynamics 2006*, pages 401–406. Springer, 2009.